Supplementary Material and Figures

Nutrient transport suggests an evolutionary basis for charged archaeal surface layer proteins

Po-Nan Li *et al.*

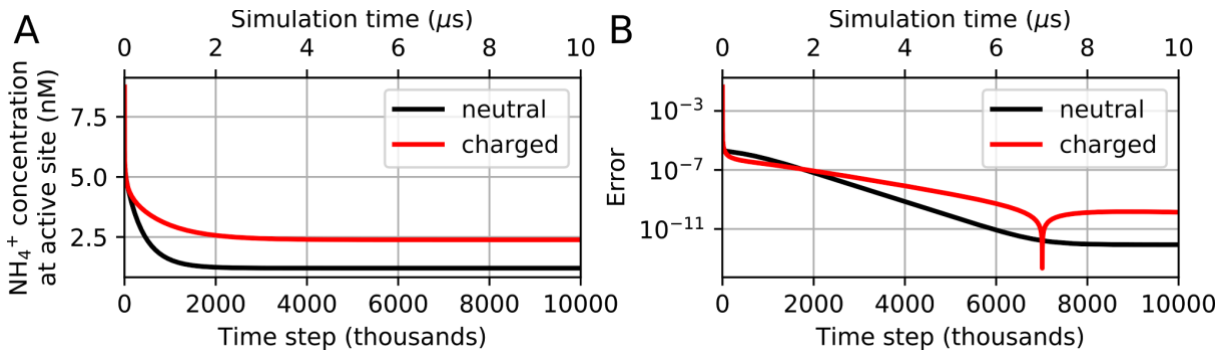

Supplementary Figure S1. Numerical convergence of the simulation. We monitored the difference of the numerical solution of the concentration at the active site between two consecutive time steps, and observed an error rate less than 10^{-4} within 1,000 time steps. (A) The evolutions of NH_4^+ concentration at the active site over simulation time; the plot shows that the simulation converges to a steady-state. (B) The error, defined as $\epsilon = |(c^{(t)} - c^{(t-1)})/c^{(t-1)}|$, is monotonically decreasing over time. The local minimum around 7000 steps reflects asymmetric convergence of the ion species (Fig S4B).

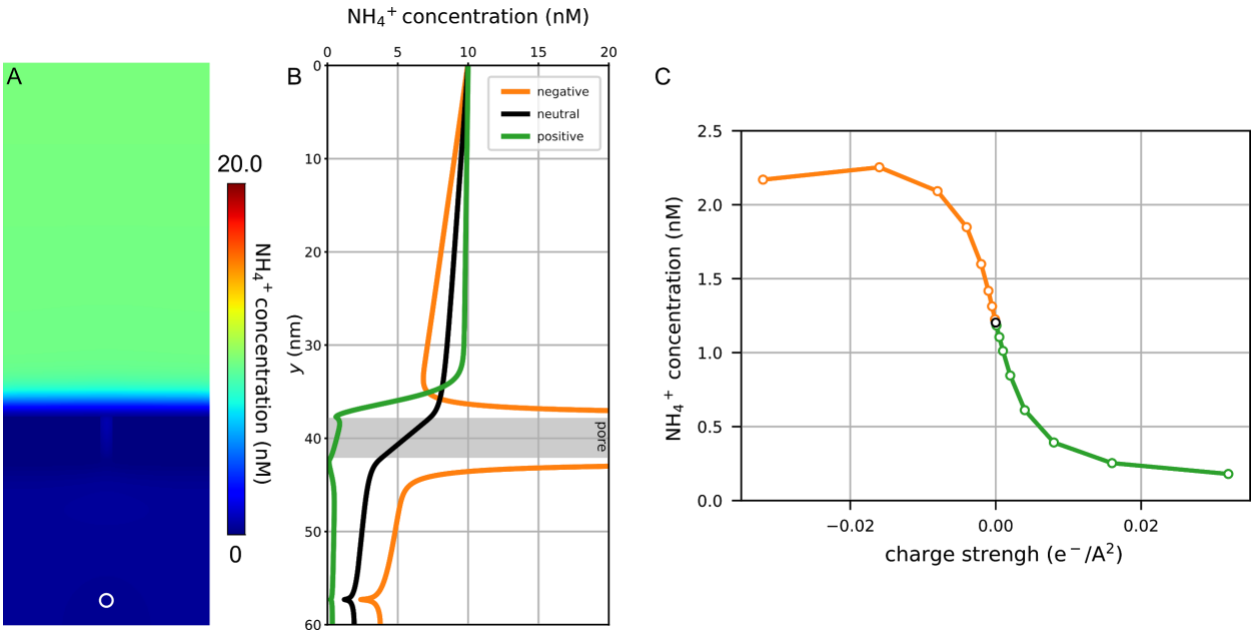

Supplementary Figure S2. Comparative NH_4^+ concentration profiles in the simulation domain with a negatively, neutral, and positively charged S-layer. (A) NH_4^+ concentration profile with a positively charged S-layer, resulting in sharply lower NH_4^+ concentration in the PPS. (B) NH_4^+ concentration profiles for neutral and charged S-layers across the length of the simulation domain at the x-location of the active site. NH_4^+ concentrations in the PPS with a positively charged S-layer are an order of magnitude lower than those with a negative S-layer. (C) NH_4^+ concentration at the active site as a function of the surface charge density of the S-layer. The black data point indicates no surface charge.

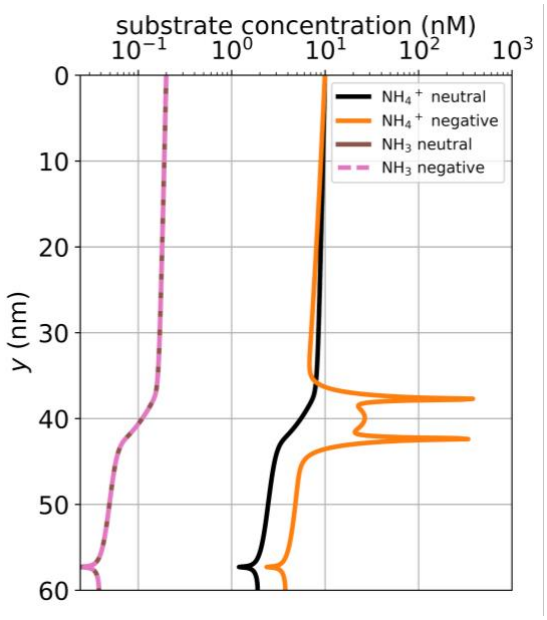

Supplementary Figure S3 Concentration profiles of NH_3 and NH_4^+ throughout the simulation domain for a neutral and negatively charged S-layer at steady state. The concentration of NH_4^+ is not affected by a neutral S-layer (black line), resulting in a reduced concentration at the active site compared to a charged S-layer (orange line). The concentration of NH_3, which is not charged, is not modulated by a charged S-layer. At pH = 7.5, NH_4^+ dominates total ammonia (NH_3+NH_4^+) bulk concentration, with corresponding NH_3 bulk concentration of just 0.2 nM. Active site NH_3 concentration is sharply reduced to 24 pM (brown and pink lines).

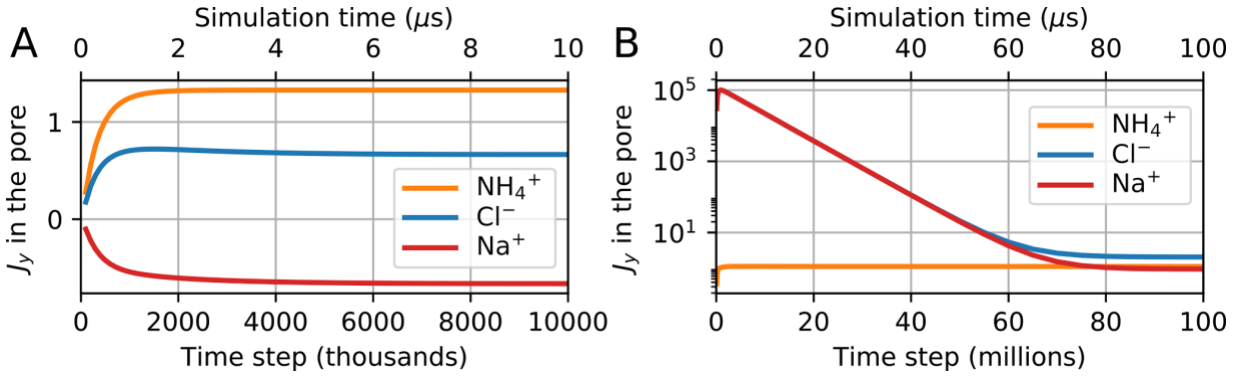

Supplementary Figure S4. Fluxes (J_y [M $m^{-2}\mu s^{-1}$]) of NH4+ (orange), Cl- (blue), and Na+ (red) through the nanopore as a function of time. Fluxes were measured in the middle of the channel. A) For a neutral S-layer, co- and counterion fluxes converge to finite values at steady state. B) For a charged S-layer, co- and counterion fluxes converged exponentially fast.

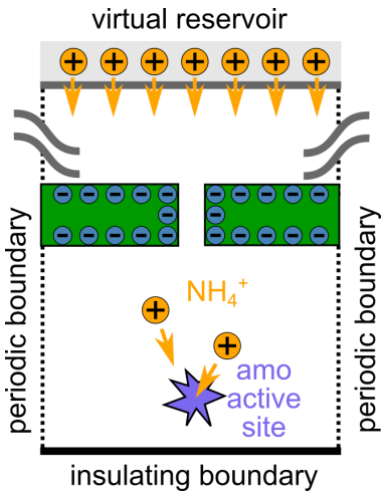

Supplementary Figure S5. Boundary conditions applied in the simulation. NH_4^+ ions reacted at the active site are compensated by adding the same amount of ions to the Dirichlet boundary condition at the top boundary.

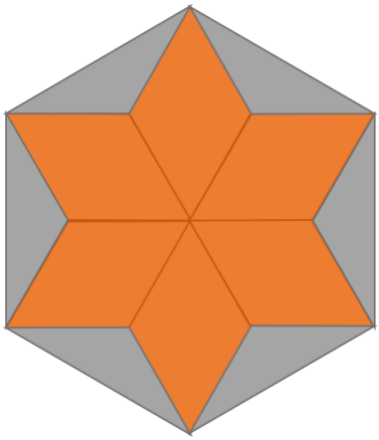

Supplementary Figure S6 Hexagonal arrangement of S-layer proteins. Each orange rhombus represents a single S-layer protein monomer, and each grey triangle represents a monomer shared with a neighboring hexagonal tile.

Supplementary Table S1. Accession numbers of archaeal S-layer gene sequences studied in this work. As most archaeal S-layer genes have not been positively identified, we selected SLP sequences based on genome annotations; however, all organisms represented have previously been observed to possess an S-layer (Albers and Meyer, 2011). The list includes virtually all known archaeal clades.

Organism	NCBI Accession
Nitrosopumilus maritimus	ABX13097
Nitrosoarchaeum limnia	EGG41144
Korarchaeum cryptofilum	WP_012310183
Thermoproteus tenax	WP_014126548
Pyrobaculum ferrireducens	AET32696
Acidianus ambivalens	CAM84437
Metallosphaera sedula	ABP94767
Sulfolobus solfataricus	WP_014511526
Desulfurococcus amylolyticus	ACL10820
Staphylothermus marinus	AAC44118
Pyrococcus furiosus	WP_011012546
Methanothermus fervidus	ADP77870
Methanothermus sociabilis	P27374
Methanocaldococcus jannaschii	WP_010870333
Methanococcus maripaludis	ABR66257
Ferroglobus placidus	ADC66245
Archaeoglobus fulgidus	WP_048095595
Picrophilus torridus	WP_011177134
Halobacterium salinarum	AAA72185
Haloferax volcanii	WP_013035656
Haloquadratum walsbyi	CCC39200
Methanosarcina acetivorans	WP_011020873
Methanosarcina mazei	CAA54899
Methanospirillum hungatei	WP_011447800
Methanoculleus marisnigri	ABN58121

Supplementary Table S2. Total potential (V) in Volts over the nanopore, current (I) in Amperes, and conductance (G) in Siemens for a neutral and charged S-layer for each of the ion species.

			NH_4^+ only		Cl^- only		Na^+ Only		Combined	
	NH_4^+ conc.	V	I	G	I	G	I	G	I	G
Neutral	10 nM	6.7E-12	-1.7E-20	-2.5E-09	8.3E-21	1.2E-09	8.3E-21	1.2E-09	5.7E-30	8.5E-19
	100 nM	7.1E-11	-1.7E-19	-2.3E-09	8.3E-20	1.2E-09	8.3E-20	1.2E-09	-9.4E-29	-1.3E-18
	1000 nM	6.7E-10	-1.6E-18	-2.4E-09	-1.6E-18	-2.4E-09	8.1E-19	1.2E-09	8.8E-27	1.3E-17
Charged	10 nM	-2.4E-11	3.3E-20	1.3E-09	-1.6E-20	-6.7E-10	-1.6E-20	-6.7E-10	1.5E-27	6.3E-17
	100 nM	-2.7E-10	3.3E-19	1.2E-09	-1.6E-19	-6.0E-10	-1.6E-19	-6.0E-10	1.6E-27	5.8E-18
	1000 nM	-2.8E-09	3.2E-18	1.1E-09	-1.6E-18	-5.7E-10	-1.6E-18	-5.6E-10	-1.9E-26	-6.7E-18

Supplementary Methods

SLP glycosylation by mass spectrometry. Cell lysate from cultures in late exponential growth was collected after mechanical lysis in a urea lysis buffer (9 M urea; 20 mM HEPES, pH 8.0). Lysate was submitted for proteomic analysis at the Vincent Coates Foundation Mass Spectrometry Laboratory, Stanford University Mass Spectrometry (http://mass-spec.stanford.edu). Briefly, proteins were crashed with acetone, centrifuged, and the protein pellet dried, reduced, and alkylated. Following a trypsin digest, peptides were column-purified and injected onto a Waters NanoAquity Ultra Performance Liquid Chromatography instrument. The mass spectrometer was a Orbitrap Elite, and resulting data was searched using Byonic (Protein Metrics) and processed using Matlab and Excel to display proteins and the number of peptides associated with them. N-linked glycosylation searches were performed with 2D posterior error probability (PEP 2D) cutoff of 10^{-4}.

Supplementary Note. In the neutral and charged S-layer case, the point-like ion sink performs work to move NH_4^+ ions across the nanopore, increasing their electrical potential. The flux of positive charges creates a negatively (upward) oriented electric field. In turn, Na^+ and Cl^- migrate along their (small) electrical-chemical gradients in the pore. The redistribution of electrical charge and chemical potential creates fluxes of Na^+ and Cl^- ions over the domain boundary. An infinitesimally small flux of co- and counterions will persist. The effect of excess or lack of co- and counterions accumulates around the point-like ion sink.